Journal of Materials Chemistry C

PAPER

View Article Online
View Journal | View Issue

Cite this: J. Mater. Chem. C, 2015, 3, 2266

Smectic A–hexagonal columnar–B7 phase transition of acute-angle bent-core molecules†

Eun-Woo Lee, Masaya Hattori, Fumiya Uehara, Masatoshi Tokita, Susumu Kawauchi, Junji Watanabe and Sungmin Kang*

Received 28th November 2014
Accepted 14th January 2015

DOI: 10.1039/c4tc02723j

www.rsc.org/MaterialsC

Acute-angle bent-shaped molecules comprising a 1,7-naphthalene central core, alkylthio terminal chains and long side wings comprising three phenyl rings connected by imine and ester linkages were synthesised. Their distinct mesomorphic properties and phase structures were revealed. Despite their acute shape, these molecules exhibited a polar switchable hexagonal columnar phase (Col_h), banana B7 phases and calamitic smectic A (SmA) phase, enabling the first observation of SmA–Col_h–B7 and Col_h–B7 phase transition behaviours. The formation of a hexagonal columnar phase between the layered smectic A and B7 phases supports the proposed Col_h phase model in which a tube-like assembly incorporating smectic layers generates hexagonal columns. Molecular packing in the optically uniaxial SmA phase was also discussed in terms of birefringence. Overall, the structural transformation of one-dimensional SmA layers into deformed hexagonal columnar and B7 phases was found to depend on the combined effects of molecular asymmetry, alkylthio terminal tails and the balance between flexible chain lengths and rigid mesogenic units.

Introduction

The correlation of mesomorphic property and molecular shape is intriguing. The mesomorphic behaviour of conventional liquid crystal (LC) mesogens such as rod-like and disk-like molecules has been widely investigated and has witnessed remarkable applications in the LC-display industry. Initially considered as non-conventional mesogens,[1] bent-shaped molecules have recently attracted extensive attention because of their interesting LC properties, such as ferroelectricity, spontaneous chirality and nonlinear optical properties, and the emergence of novel phases called B1–B7 banana phases.[2–6] The enhanced molecular packing along the bent direction in banana phases has been proposed as a main factor for polarity, suggesting that the molecular bend angle plays an important role in promoting these phases. A bend angle approximating 120° usually leads to unique mesomorphism in banana phases.[2] Typical central-core units such as 1,3-disubstituted benzenes, 2,6-disubstituted pyridines, 2,7-disubstituted naphthalenes and 1,3-disubstituted biphenyls exhibit a bend angle ranging from 110° to 140°, which is recognized as favourable for banana phases.[7,8] In contrast, some studies have addressed molecules in which central cores display an acute bend angle (<90°), such as 1,2-disubstituted benzenes and 2,3-disubstituted naphthalenes, because these molecules tend to form calamitic mesophases.[9–11] However, interestingly, recent studies have revealed that acute-angle bent-core mesogens comprising a 1,7-naphthalene central core formed the well-known B4 banana phase and polar switchable smectic A phases (SmAP).[12,13] In addition, hexagonal columnar (Col_h) and cubic (Cub) phases have been discovered in bent-core LC systems,[14–16] consistent with molecular packing in the bent direction, even with a bending angle of 60°. Understanding molecular orientation in these mesophases remains challenging, in particular whether the bent direction is parallel or perpendicular to the layer normal in smectic phases and the *n*-director in nematic phases. One controversial example is related to acute-angle bent-core molecules comprising a 2,3-naphthalene core with ester-type side wings. These molecules have been reported as switchable by Choi *et al.*[17,18] but non-switchable by Ros *et al.*[19,20] in the smectic phase. Thus, we believe a species of acute-angle bent-core mesogens can be an ultimate example that lies on the line between the banana-like and calamitic LC properties.

In this study, asymmetric bent-shaped molecules comprising a 1,7-naphthalene central core (N(1,7)), alkylthio terminal chains (S) and long side wings comprising three phenyl rings connected by imine (I) and ester linkages (E) were prepared (Scheme 1) which possess a longer mesogenic unit length compared with our previous report.[14,16] Their mesomorphic properties as a result of extension of the mesogenic part, including their molecular accommodation within the LC phase, were investigated. The

Department of Organic and Polymeric Materials, Tokyo Institute of Technology, Ookayama, Meguro-ku, Tokyo 152-8552, Japan. E-mail: skang@polymer.titech.ac.jp; Fax: +81-3-5734-2888; Tel: +81-3-5734-3641

† Electronic supplementary information (ESI) available: Fig. S1. POM micrographs of SmA and B7 phases. Fig. S2. Transmittance spectrum and obtained birefringence of SmA. Synthetic procedure and NMR analysis data. See DOI: 10.1039/c4tc02723j

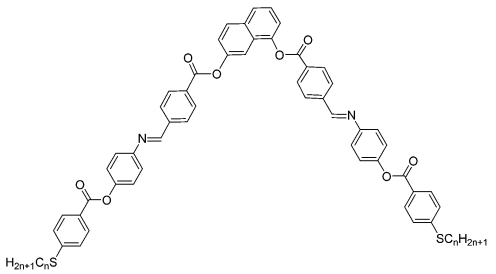

Scheme 1 Chemical structure of N(1,7)–EIE–S*n* (n = 16, 18, 20).

V-shaped mesogens are designated as N(1,7)–EIE–S*n* (n = 16, 18, 20), where n denotes the number of carbon atoms in the terminal alkylthio tails.

Results and discussion

Differential scanning calorimetry (DSC) thermograms, along with transition temperatures and associated enthalpies, are shown in Fig. 1 and Table 1 for N(1,7)–EIE–S*n* (n = 16, 18, 20). At a glance, all thermograms similarly displayed isotropisation points over 250 °C and three exothermic peaks upon cooling. However, additional small peaks were observed approximately at 240 °C–250 °C only for n = 16 and 18. This difference was visible by polarized optical microscopy (POM). Upon cooling of the isotropic melt at 5 °C min^{-1}, N(1,7)–EIE–S16 exhibited a typical fan-shape texture at 240 °C (Fig. 2a), which indicates a smectic A (SmA) phase. Upon further cooling, this fan-shape texture changed to a broken fan-like texture at 220 °C (Fig. 2b). A similar transformation from a typical fan-shape texture to a broken fan-like texture was also observed for N(1,7)–EIE–S18 (Fig. 2d and e). When further cooled, these broken fan-like textures (Fig. 2b and e) turned into dark fringed patterns with weakened birefringence (Fig. 2c and f). On the other hand, N(1,7)–EIE–S20, which contained the longest alkylthio chains, exhibited a rather simple phase sequence. Upon cooling, its isotropic melt generated a typical mosaic texture at 240 °C (Fig. 2g), consistent with the columnar ordering of the mesophase. Next, this mosaic texture coalesced into a fringed pattern at 195 °C (Fig. 2h). Although the birefringence of this pattern (Fig. 2h) was slightly higher than that for N(1,7)–EIE–S16 (Fig. 2c) and N(1,7)–EIE–S18 (Fig. 2f), all fringed patterns looked similar. All three compounds underwent crystallisation upon further cooling. The resulting phase sequence properties are given in Fig. 1d. LC phases include SmA, hexagonal columnar and banana B7 phases (see the discussion below).

Phase structures in all LC regimes were examined in detail by synchrotron radiation (SR) wide-angle X-ray diffraction (WAXD) and small-angle X-ray scattering (SAXS) because temperature-resolved SR X-ray measurements effectively detect subtle phase transition sequences presenting narrow LC regimes and relatively high transition temperatures. Fig. 3 shows representative two-dimensional (2D) powder SAXS profiles for each phase as well as one-dimensional (1D) powder SAXS and WAXD profiles for N(1,7)–EIE–S18. Table 2 lists observed and calculated

Table 1 Phase transition properties of N(1,7)–EIE–S*n*

Compound	Temperature[a]/°C (enthalpy[a]/kJ mol^{-1})
N(1,7)–EIE–S16	Cr 201(31.4) B7 210(9.7) Col_h 240(0.6) SmA 258(4.7) Iso, T_m: 207
N(1,7)–EIE–S18	Cr 195(31.3) B7 204(8.9) Col_h 250(0.2) SmA 256(4.2) Iso, T_m: 203
N(1,7)–EIE–S20	Cr 193(29.9) B7 202 (8.3) Col_h 260(7.3) Iso, T_m: 202

[a] Determined by the cooling process. T_m: melting point, Iso: isotropic phase, Cr: crystal phase.

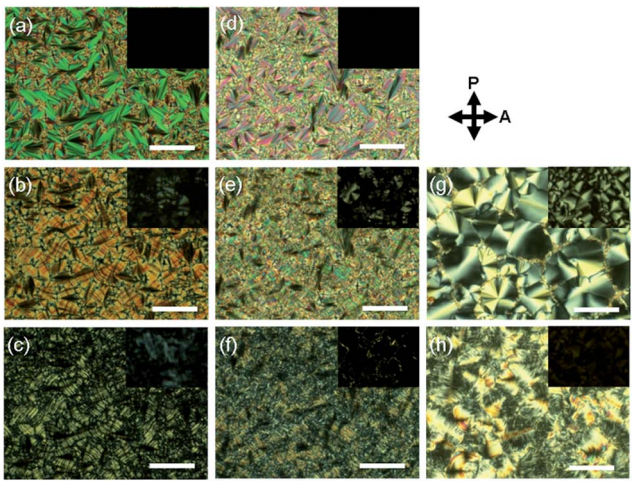

Fig. 2 POM textures observed under glass cells treated with a polyimide planar alignment layer without rubbing treatment. Insets are textures obtained with a homeotropic alignment: (a) SmA at 250 °C, (b) Col_h at 220 °C, (c) B7 phase at 200 °C for N(1,7)–EIE–S16; (d) SmA at 245 °C, (e) Col_h at 220 °C, (f) B7 phase at 195 °C for N(1,7)–EIE–S18; (g) Col_h at 240 °C, (h) B7 phase at 195 °C for N(1,7)–EIE–S20. The scale bar indicates 100 μm.

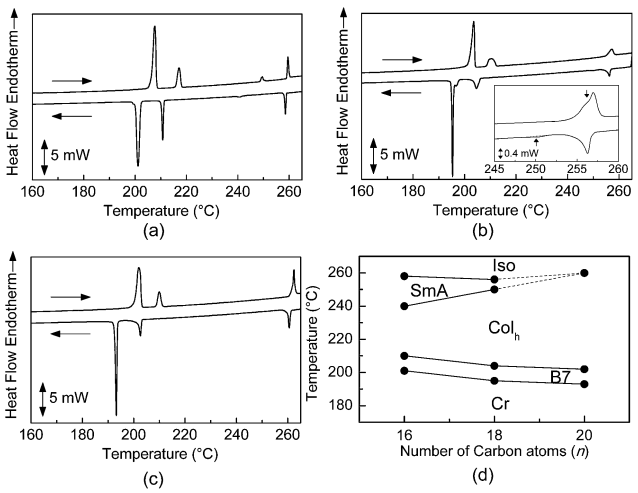

Fig. 1 Heating and cooling DSC thermograms of N(1,7)–EIE–S*n*: (a) n = 16, (b) n = 18 and (c) n = 20 with a scanning rate of 5 °C min^{-1}. (d) Phase transition behaviours of N(1,7)–EIE–S*n* as a function of the terminal carbon numbers.

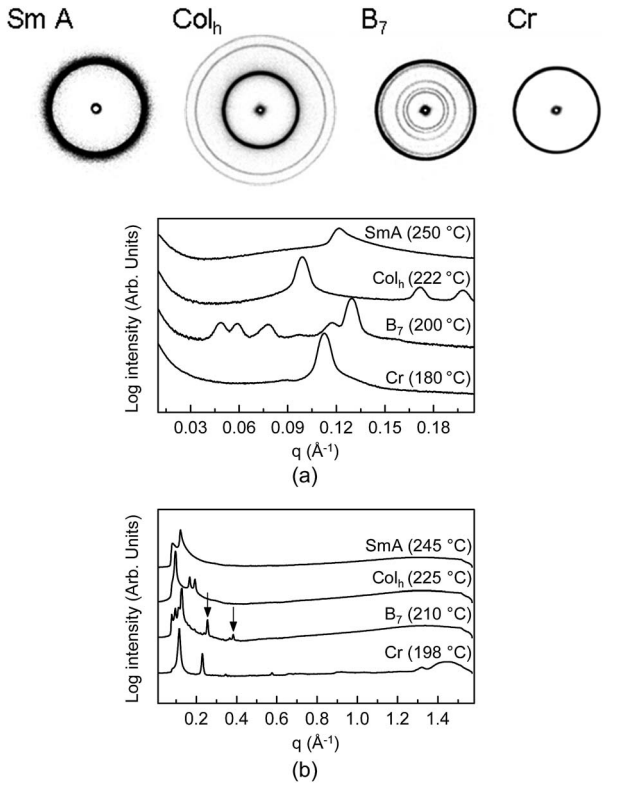

Fig. 3 X-ray investigations of the powder sample for N(1,7)–EIE–S18. (a) 2D and 1D SAXS profiles and (b) 1D WAXD profile obtained from each phase.

Table 2 X-ray data and lattice parameters for N(1,7)–EIE–S*n*

Compound	Phase	d_{obs}[a] (Å)	hkl[b]	d_{calc}[b] (Å)	Lattice parameter[b]
N(1,7)–EIE–S16	SmA	49.5	001		
	Col$_h$	62.4	100	62.4	a = 72.1 Å
		36.1	101	36.1	
		31.2	200	31.2	
	B7	132.8	201	132.7	a = 296 Å,
		102.6	100	102.7	c = 133 Å,
		87.3	301	85.7	β = 20.3°
		77.8	101	77.4	
		51.8	200	51.3	
		46.2	001	46.3	
	Cr	53.0	001		
N(1,7)–EIE–S18	SmA	52.3	001		
	Col$_h$	64.5	100	64.5	a = 74.5 Å
		37.0	101	37.2	
		32.1	200	32.2	
	B7	135.9	201	135.6	a = 300 Å,
		106.4	100	106.5	c = 136 Å,
		87.5	301	87.2	β = 20.8°
		81.0	101	80.7	
		53.5	200	53.3	
		48.3	001	48.3	
	Cr	56.1	001		
N(1,7)–EIE–S20	Col$_h$	64.5	100	65.0	a = 75.0 Å
		37.0	101	37.5	
		32.1	200	32.5	
	B7	119.4	201	119.2	a = 259 Å,
		110.4	100	110.4	c = 119 Å,
		81.8	101	82.5	β = 25.2°
		55.2	200	55.2	
		50.8	001	50.8	
	Cr	58.5	001		

[a] Observed *d*-spacings upon cooling. [b] Calculated Miller indices *hkl*, *d*-spacings and lattice parameters with 2D hexagonal and oblique lattices.

d-spacings, Miller indices and lattice parameters. Upon cooling of the highest-temperature LC phase, a single reflection appeared at $2\pi/49.5$ and $2\pi/52.3$ Å^{-1} for N(1,7)–EIE–S16 and N(1,7)–EIE–S18, respectively, in addition to an outer diffraction peak at $2\pi/4.7$ Å^{-1}, implying that the corresponding phases exhibit a 1D lamellar order consistent with a smectic A phase. Upon cooling of N(1,7)–EIE–S18 to the lower temperature phase, this single reflection propagated into three sharp reflections at $2\pi/64.5$, $2\pi/37.0$ and $2\pi/32.1$ Å^{-1}. These reflections were incommensurable but showed ratios of 1, $3^{-1/2}$ and 2^{-1} with the *d*-spacings and were eventually indexed to (100), (101) and (200), respectively. These ratios were clearly indexed and matched a hexagonal columnar lattice structure (Table 2), in which one lattice edge amounted to 72.1 and 74.5 Å for N(1,7)–EIE–S16 and N(1,7)–EIE–S18, respectively. A similar scattering pattern was observed for N(1,7)–EIE–S20. Upon cooling of the isotropic melt, the observed *d*-spacings of 65.0, 37.4 and 32.5 Å gave a lattice parameter of 75.0 Å comparable to the size obtained for N(1,7)–EIE–S18. These reflection profiles provide hexagonal ordering parameters that significantly exceed the molecular length, in agreement with previously observed hexagonal columnar phases formed by acute-angle banana-shaped derivatives bearing the 1,7-naphthalene core and five rings.[14–16] Scattering patterns changed more drastically when the compounds were cooled to their lowest-temperature LC phase. In addition to a wide-angle diffuse scattering at $2\pi/4.7$ Å^{-1}, five or six additional reflections were recorded in the small angle region (Fig. 3 and Table 2). Together with the low birefringence and fringed textural transformation detected by POM, these observations suggest that long-range frustration occurs in the smectic phases with a periodicity of approximately 300 Å. This low-temperature phase was determined as a banana B7 phase showing a 2D long-range frustrated/undulated structure. For N(1,7)–EIE–S18, the indexation of peaks at 135.9, 106.4, 87.5, 81.0, 53.5 and 48.3 Å led to (201), (100), (301), (101), (200) and (001) reflections, respectively, consistent with the formation of a 2D lattice presenting parameters a of 300 Å, c of 136 Å and β of 20.8°. This indexation also matched with the observed *d*-spacings for n = 16 and 20 and indicated the emergence of oblique 2D lattices in these homologues (Table 2). Furthermore, higher-order reflections of (002) and (003) corresponding to q values of $2\pi/24.2$ and $2\pi/16.1$ Å^{-1} (see arrows in Fig. 3b) were found as a result of layer order, indicative of a well-defined layer structure in this phase.

These interpretations were strongly supported by X-ray investigations using oriented samples. Fig. 4 shows oriented SAXS patterns observed in SmA, Col$_h$ and B7 phases upon cooling of homeotropically aligned N(1,7)–EIE–S16. First, a simple (001) reflection was visible along the meridional line in

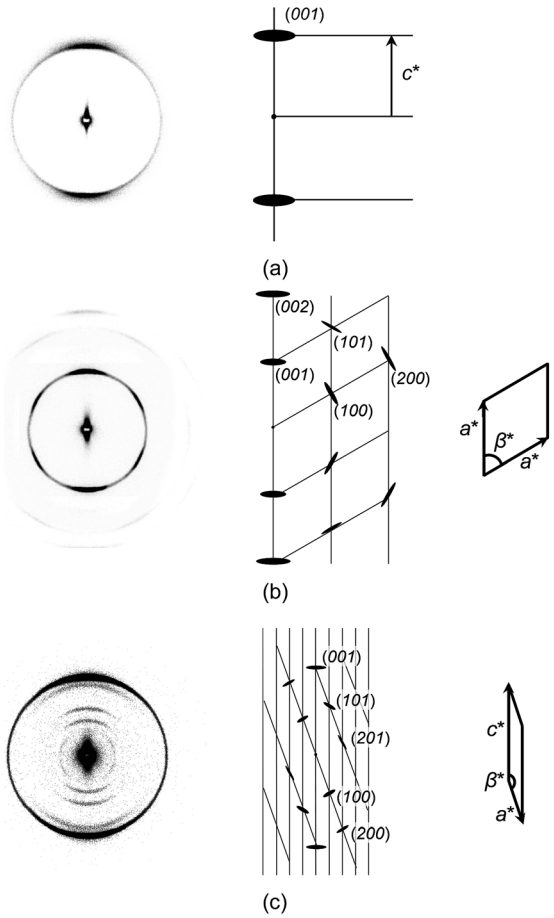

Fig. 4 2D oriented SAXS patterns of (a) SmA, (b) Col_h and (c) B7 phases for N(1,7)–EIE–S16 obtained from the homeotropically aligned sample on a glass plate. The X-ray beam is irradiated along the direction parallel to the glass plate which was set along the equatorial line. The right-hand side of each figure shows the resulting reciprocal space and lattices which are interpreted as 1D layer, hexagonal and 2D oblique structures, respectively.

the SmA phase, consistent with a 1D layer order (Fig. 4a). A drastic change was clearly detectable in the Col_h phase. As can be seen from Fig. 4b, six spot-like reflections for (100), (101) and (200) were distinguished, in agreement with the *d*-spacing relationships and the typical directions of the scattering vectors, providing a hexagonal lattice assembly with an edge size a of 72.1 Å. Upon further cooling, this oriented profile evolved into a rather complicated pattern displaying several split and streak sets along the meridional line (Fig. 4c), suggesting a 2D frustrated B7 phase structure in an oblique lattice (lattice parameters, $a = 296$ Å, $c = 133$ Å and $\beta = 20.3°$). Indices and reciprocal lattices are given on the right-hand side of each plot (Fig. 4). Moreover, lattice parameters did not show any temperature dependence within 9 °C of the B7 phase regime, consistent with long-range periodicity.

The six spot-like scattering patterns observed for the columnar phase may also be interpreted as a frustrated B1 structure.[4,21,22] In this case, two of the smallest reflections located on the meridional line and the other four spots would be indexed as (002) and (101), respectively. However, this merely happens when the *d*-spacing values for (002) are equivalent to those of the (101) reflection, which seems occasional and usually occurs when *d*-spacings change as a result of molecular length tuning, particularly variations in the terminal carbon chain number. A disagreement between *d*-spacing values when n varies would rule out a B1-like phase. Here, the *d*-spacings obtained for the inner six spots consistently amounted to 62.4, 64.5 and 65.0 Å for $n = 16$, 18 and 20, respectively. Furthermore, the observed *d*-spacing value for (100) or (001) was larger than half the estimated molecular length but smaller than double this length.

Electro-optical measurements were performed to investigate the polar switching ability of SmA, Col_h and B7 phases. No polar switching behaviour was detected in the SmA phase for N(1,7)–EIE–S16 and N(1,7)–EIE–S18. On the other hand, Col_h and B7 phases showed distinct switching behaviours in the presence of an external field for all three compounds. Fig. 5 and 6 show representative examples of switching in Col_h and B7 phases for N(1,7)–EIE–S20. Under an applied triangular voltage exceeding 89.5 V_{pp} μm^{-1}, the mosaic-like Col_h phase (Fig. 5a) coalesced into a totally dark texture (Fig. 5b), concomitant with a single reversal current within a half period of the triangular wave (Fig. 5c). This result agrees with previous reports on a polar hexagonal columnar phase for five-ring 1,7-naphthalene derivatives, albeit at a remarkably elevated threshold voltage.[14,15] Consistent with X-ray measurements, these observations suggest that the hexagonal columnar phase presents a ferroelectric switching behaviour. In this phase, the columns may reorient parallel to the field direction as a result of the collective motion of constituent molecules (here, the direction of cell thickness), resulting in an optically isotropic state.[14,15]

The B7 phase showed a ferroelectric switching behaviour at a lower threshold voltage of 24.8 V_{pp} μm^{-1} than the Col_h phase in addition to a single reversal current within a half period of the

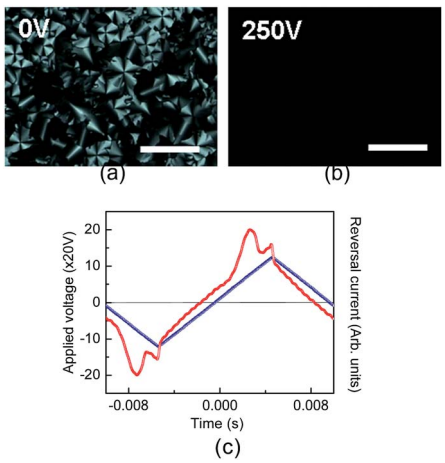

Fig. 5 Electro-optic properties of Col_h phase for N(1,7)–EIE–S20 measured at 210 °C: (a) an optical microscopic mosaic and circular texture with low birefringence was observed upon cooling from the isotropic melt; (b) optically isotropic texture obtained under the applied electric field; (c) polarization reversal current during the application of triangular wave voltage (500 V_{pp}, cell gap: 3.5 μm, 50 Hz). pp denotes peak-to-peak. The scale bar indicates 100 μm.

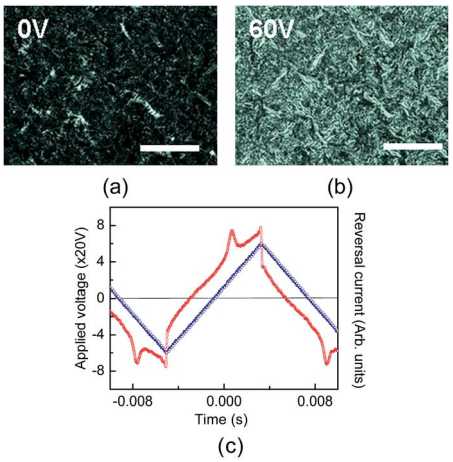

Fig. 6 Electro-optic properties of the B7 phase for N(1,7)–EIE–S20 measured at 195 °C: (a) dark fringed texture was observed before applying the electric field; (b) birefringence change observed under the applied electric field; (c) polarization reversal current under the application of triangular wave voltage (240 V_{pp}, cell gap: 3.5 μm, 60 Hz). The scale bar indicates 100 μm.

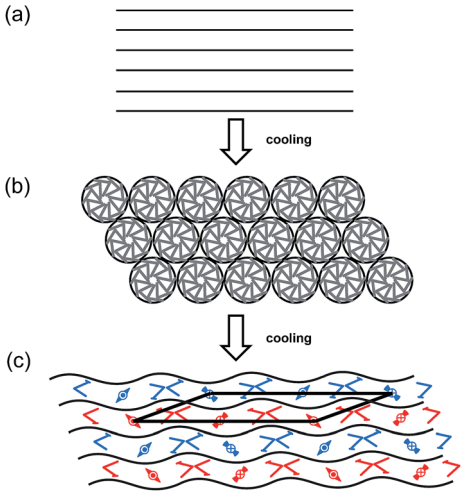

Fig. 7 Illustration of possible structural transformation occurring at the SmA–Col_h–B7 phase transition based on the observation of oriented X-ray scattering patterns in case of without external field. (a) 1D layering order of SmA phase, (b) hexagonal ordering of columns composed of a tube-like assembly of enclosed layers and (c) anticlinic ferroelectric layer ordering of the B7 phase with layer undulation that provides a 2D oblique lattice. This is one possible polar structure in case that the layer chirality is homochiral within one layer. Here, the (00*l*) planes of the hexagonal lattice in (b) and 2D oblique lattice in (c) have the same direction parallel to the equatorial line.

triangular wave (Fig. 6). In the presence of an applied external field, the initial low-birefringence texture (Fig. 6a) was transformed into a rather bright texture (Fig. 6b) which persisted after the field was turned off. Overall, the lowest-temperature LC phase was therefore designated as the B7 phase (especially a switchable B7 phase was expressed as B7′),[6] which typically is a polar switchable phase exhibiting 2D long-range frustration/undulation. Polar switching was thought to stem from the collective reorientational motion of molecular assemblies packed along the bent direction in the B7 phase layers. Spontaneous polarizations (P_s) approximated 120–200 and 240–300 nC cm^{-2} for the Col_h and B7 phases, respectively, comparable with previous values for the Col_h phase.[14,15] A possible model is proposed for the hexagonal columnar phase using X-ray and electro-optical results. Here, for a hexagonal lattice edge a of 75 Å, a stratum height h of 4.7 Å in each column and a density ρ of 1 g cm^{-3}, the average number of molecules N amounted to 10, in close agreement with previous observations. Thus, this hexagonal model may involve tube-like columns of cylindrically enclosed layers, as previously suggested.[14,16]

Here, the appearances of a flat, layered calamitic SmA phase and a frustrated layered B7 phase on either side of the upper- and lower-temperature regions of the Col_h phase should be addressed. In general, a hexagonal phase lacks layer order, such as in a disc-like arrangement. Therefore, it seems unlikely between two layered phases as in our case because the layer structures would require a significant amount of energy to form and disassemble. However, to the best of our knowledge, the SmA–Col_h–B7 phase transition sequence is the first observed in bent-core mesogenic systems. This sequence supports our interpretation of a hexagonal columnar structure suggesting an assembly of tube-like columns containing concentrically enclosed layers.

A possible model for the structural propagation during the cooling process is proposed in Fig. 7. The 1D layering (Fig. 7a) breaks down into hexagonal columns of enclosed layers *via* layer bending (Fig. 7b), which may result from the asymmetric shape of the molecular centre during molecular packing along its direction. Upon further cooling, the hexagonal structure rearranges into the B7 phase exhibiting undulated layers, in which the polarization splay defect lines separate smectic blocks of opposite molecular tilt directions (Fig. 7c).[23]

First, polar properties observed in the Col_h and B7 phases presented a strong evidence for molecular packing states in each LC phase, which indicates a banana-like molecular packing. Therefore, packing along the molecular bent direction was effectively enhanced although the bent-core mesogens displayed an acute angle of approximately 60°.

Second, let us identify the molecular packing states dominating the SmA phase. The optically isotropic POM textures for homeotropically aligned mesogens in the SmA phase demonstrate an optical uniaxiality within visible light wavelengths (insets in Fig. 2a and d). Therefore, the SmA phase may be considered a calamitic smectic phase often observed in conventional rod-like LC molecules. However, U-shape (or U-like)[24–26] and banana-shape (or banana-like)[27–29] molecular arrangements are possible when the molecular bend direction is parallel or perpendicular to the layer normal, respectively (Fig. 8).

Information about molecular packing in the smectic layer was obtained by optical investigations. The SmA phase showed birefringence in which the long axis of the refractive index ellipsoid lay parallel to the long axis of the fan-shape domain by POM,[30] which is converse in the B7 phase.[31] This implies that the layer normal direction presents a larger refractive index

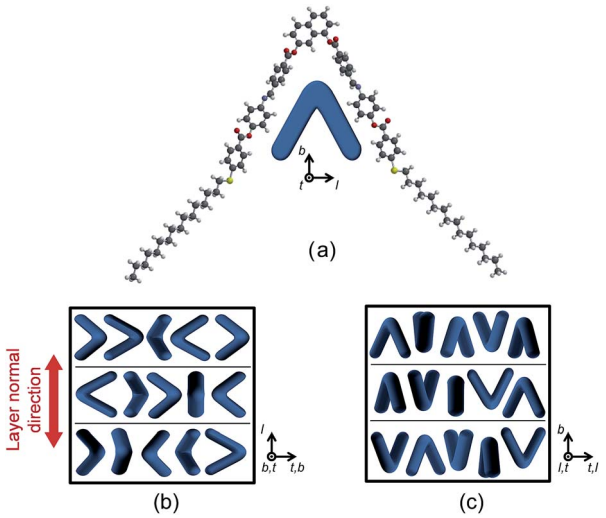

Fig. 8 (a) Optimized molecular structure of N(1,7)–EIE–S16 and set of three axis on the molecular scheme. Here, b, l and t denote bent, longitudinal and transversal, respectively. Two possible models of uniaxial SmA phase in which the bent direction is either (b) perpendicular (model 1) to layer normal or (c) parallel to it (model 2).

than the layering direction. The V shape of the N(1,7)–EIE–S*n* molecules made the molecular bend axis exhibiting the largest refractive index value difficult to identify. Therefore, the polarisability (α) was calculated along the three axes determined on the optimized molecular structure (Fig. 8a).[34–36] Then, the values of $\alpha_{b,l,t}$ were converted into refractive indices of n_b, n_l and n_t that eventually gave the values of n_e, n_o and birefringence (Δn, when order parameter $S = 1$) in Table 3. Here, the subscripts b, l and t denote bend, longitudinal and transversal directions, respectively. Assuming that the uniaxial SmA phase adopted two geometries, in which the bend direction was either perpendicular (Fig. 8b, model 1) or parallel to the layer normal (Fig. 8c, model 2), the birefringences (Δn at 550 nm) for two models considering order parameter values $S = 0.4$–0.6 were derived as 0.002–0.004 and 0.116–0.173, respectively (here, surface effects were ignored and the extraordinary axis was set parallel to the layer normal). These calculations firstly showed that the refractive index along the bend direction n_b displayed the largest value as we expected. Secondly, the expected Δn values considering practical order parameter values in the SmA phase are both small but especially quite low for model 1. In order to confirm these optical performance, we performed a birefringence measurement[28,32,33] and obtained $\Delta n' = 0.114$ (at 550 nm, $'$ denotes a value obtained by experimental observation)[37] for N(1,7)–EIE–S16, which was in good agreement with the calculated birefringence (Δn) for model 2. However, the observed layer thickness (48.3 Å) for N(1,7)–EIE–S16 was rather comparable with the molecular length corresponding to the end-to-end distance between terminal chains (51.3 Å) but larger than the molecular height (34.5 Å, length of the perpendicular line measured between the apex of the central core and the base of the triangle) with the most extended terminal chain conformer.[34] Therefore, it is difficult to assert that the single molecular length in a U-shaped conformation and packing satisfies the observed layer thickness. Overall, molecular packing in the uniaxial SmA phase remains unclear although the observed birefringence suggests that molecules adopt U-shaped packing irrespective of the deviation in the layer thickness.

The formation of layered mesophases and the Col_h phase between these layered phases indicate that this Col_h phase might originate from columns of cylindrically enclosed smectic layers instead of the disc-like molecular association of columns although the reason for the low values of transition enthalpies in the SmA–Col_h phase transition remains unclear. Because of the flexibility of terminal alkyl chains and the valence between mesogens and terminal chain lengths in asymmetric structures, smectic A-to-columnar phase transitions have been reported in coil–rod–coil systems[38,39] and bolaamphiphiles.[40] Consequently, the balance between terminal chains and mesogens, the rotational freedom of the alkylthio linkage[41] and symmetric structure of the N(1,7)–EIE–S*n* system may promote their transition motion, resulting in a replacement of the SmA phase with the columnar phase upon terminal chain lengthening. The current observation, in addition to our previous observations of cubic, Col_h, X, B7 and B2 phases,[14,16,42] might be explained by a relationship between layer elastic constants and temperature. In the lowest temperature region, the liquid banana phases (B2 and B7) reside stably due to the effective molecular packing along the bent direction; however, by increasing the temperature, the layer begins to deform due to reduced layer elastic constants or weakened packing correlation along the bent direction, resulting in Col_h, X and Cub phases. Finally, for the uniaxial SmA phase, a rebuilding of layer order appearing in the highest temperature region can be understood as a form that has a different molecular accommodation from that of the preceding phase, *i.e.* a U-shaped packing and 1D layer structure free of layer strain.

Table 3 Calculated polarisability, refractive indices and birefringences for two geometries in the uniaxial SmA phase for N(1,7)–EIE–S16

	Polarisability (Bohr^3)			Refractive index						
λ^a (nm)	α_b	α_l	α_t	n_b	n_l	n_t	Model	n_e	n_o	Δn^b
450	1776.3	1203.3	680.2	1.812	1.596	1.369	1	1.596	1.591	0.005
							2	1.812	1.483	0.330
550	1638.3	1139.1	670.5	1.745	1.556	1.355	1	1.556	1.550	0.006
							2	1.745	1.456	0.289

[a] Wavelength applied for calculation. [b] In the case of $S = 1$, calculated by $n_l - (n_b + n_t)/2$ and $n_b - (n_l + n_t)/2$ for model 1 and model 2, respectively.

Conclusions

Bent-shaped molecules comprising a 1,7-naphthalene central core, alkylthio terminal chains and long side wings containing three phenyl rings connected to imine and ester linkages were prepared. Their mesomorphic properties and phase structures were evaluated as a function of the alkylthio tail length. Despite their acute shape, these compounds with an extended mesogenic unit exhibited polar switchable Col_h and B7 phases in addition to a non-polar SmA phase. This study showed the first examples of SmA–Col_h–B7 and Col_h–B7 phase transitions and the second instance of a banana B7 phase for a low-bend-angle molecule in addition to 1,2-phenylene derivatives.[42] This polymorphic phase transition sequence may provide a better understanding of structural properties of a hexagonal columnar phase, which was interpreted as an assembly of enclosed layers although there still remains a different interpretation, *i.e.* a disc-like column formation. Effective packing was observed in the acute-shaped bent-core molecules. Therefore, even with a critical bend angle approximating 60°, a banana phase formed in addition to calamitic LC phases. These observations and recent reports on cubic, X, Col_h and banana phases suggest that the interplay between the central core in the mesogenic unit and terminal chain lengths is extremely important for mesomorphic properties, such as the occurrence of 1D layering (SmA), layer deformations (Col_h, X and Cub phases) and banana-like packing arrangements (B2 and B7), particularly in acute-angle bent-core LC systems. Details on the uniaxial smectic phase remain unclear. However, the observed birefringence and the direct formation of the Col_h phase imply that the tube-like column structure of the Col_h phase may be an intermediate state between the smectic phase of the U-like molecular packing and the banana phases presenting effective molecular packing along the bend direction. This study demonstrated that a simple replacement of alkoxy with alkylthio chains generated an entirely different phase sequence, providing insight into the relationship between the ultimate molecular shape/design and the formation of banana LC phases.

Experimental

Synthesis and characterization

Three homologues of 1,7-naphthalene bis(4-(4-(4-(*n*-alkylthio) benzoyloxy)phenyliminomethyl)benzoate) (N(1,7)–EIE–S*n*) (n = 16, 18 and 20) were synthesised as described previously.[12,14] The general synthetic route is detailed in Scheme S1 (ESI†).[43] ^{1}H- and ^{13}C-NMR analyses were conducted using a JEOL 400 MHz NMR spectrometer for all synthesised compounds. Elemental analyses were performed using a Thermofinnigan EA1108 instrument. NMR and elemental analysis results are shown in the ESI.†[44]

Measurements

The thermal behaviour was investigated using a Pyris1 DSC instrument under a N_2 atmosphere at heating and cooling rates of 1 °C min^{-1}–10 °C min^{-1}. POM textures were observed using an Olympus BX50 optical microscope equipped with a Mettler FP 82 HT hot stage and Mettler FP 90. WAXD measurements were performed using a Bruker D8 DISCOVER diffractometer equipped with a Vantec-500 detector, and SAXS measurements were conducted using a Bruker NanoSTAR-U fitted with an X-ray generator with monochromatic CuKα radiation. Temperature-resolved SR experiments were performed at the 4C beamline of the Pohang Light Source II (PLS-II) (Pohang, Korea). Powder X-ray investigations were conducted using samples kept in 1.5 mm-diameter glass capillary tubes. Oriented pattern X-ray investigations were performed using homeotropically aligned samples obtained by slowly cooling the isotropic liquid on a glass substrate treated with an organosilane agent. Electro-optical switching behaviour was evaluated using a high-speed voltage amplifier (FLC Electronics, F20A) connected to a function generator (NF Electronic Instruments, WF 1945A). For an applied voltage exceeding 400 V_{pp}, a high-voltage amplifier (NF Electronic Instruments) was utilized. The sample was injected between indium–tin-oxide-coated glass plates. The polarization reversal current was measured by applying a triangular wave voltage. Second harmonic generation intensity was observed using the oblique incidence (45°) of a polarized fundamental wave emitted by a Q-switch Nd:YAG laser (Continuum, Surelite II 10P) onto the cell. Signals passed through appropriate optical filters before being detected with a photomultiplier tube (Hamamatsu R-955) and output signals were accumulated using a BOXCAR system (Stanford Research Systems). The Δn measurement was performed by a microscopic spectroscopic method using a Nikon LV100 Pol optical microscope equipped with a USB4000 (Ocean Photonics) spectrometer.

Acknowledgements

This work was supported by a Grant-in-Aid for Scientific Research (KAKENHI) Grant no. 26410086. Numerical calculations were conducted using the TSUBAME2.5 supercomputer at the Tokyo Institute of Technology, Tokyo, Japan. Synchrotron radiation X-ray measurements were performed using the 4C beamline at the Pohang Light Source II (PLS-II).

Notes and references

1 D. Vorländer, *Ber. Dtsch. Chem. Ges.*, 1929, **62**, 2831–2835.
2 T. Niori, T. Sekine, J. Watanabe, T. Furukawa and H. Takezoe, *J. Mater. Chem.*, 1996, **6**, 1231–1233.
3 D. R. Link, G. Natale, R. Shao, J. E. Maclennan, N. A. Clark, E. Körblova and D. M. Walba, *Science*, 1997, **278**, 1924–1927.
4 G. Pelzl, S. Diele and W. Weissflog, *Adv. Mater.*, 1999, **11**, 707–724.
5 H. Takezoe and Y. Takanishi, *Jpn. J. Appl. Phys.*, 2006, **45**, 597–625.
6 R. A. Reddy and C. Tschierske, *J. Mater. Chem.*, 2006, **16**, 907–961.
7 D. Shen, S. Diele, G. Pelzl, I. Wirth and C. Tschierske, *J. Mater. Chem.*, 1999, **9**, 661–672.

8 S. Kang, Y. Saito, N. Watanabe, M. Tokita, Y. Takanishi, H. Takezoe and J. Watanabe, *J. Phys. Chem. B*, 2006, **110**, 5205–5214.
9 H. Matsuzaki and Y. Matsunaga, *Liq. Cryst.*, 1993, **14**, 105–120.
10 M. Kuboshita, Y. Matsunaga and H. Matsuzaki, *Mol. Cryst. Liq. Cryst.*, 1991, **199**, 319–326.
11 C. V. Yelamaggad, I. Shashikala, D. S. S. Rao and S. K. Prasad, *Liq. Cryst.*, 2004, **31**, 1027–1036.
12 S. K. Lee, L. Shi, R. Ishige, S. Kang, M. Tokita and J. Watanabe, *Chem. Lett.*, 2008, **37**, 1230–1231.
13 S. K. Lee, X. Li, S. Kang, M. Tokita and J. Watanabe, *J. Mater. Chem.*, 2009, **19**, 4517–4522.
14 X. Li, S. Kang, S. K. Lee, M. Tokita and J. Watanabe, *Jpn. J. Appl. Phys.*, 2010, **49**, 1217011–1217016.
15 X. Li, M. Zhan and K. Wang, *New J. Chem.*, 2012, **36**, 1133–1136.
16 S. Kang, M. Harada, X. Li, M. Tokita and J. Watanabe, *Soft Matter*, 2012, **8**, 1916–1922.
17 E.-J. Choi, X. Cui, C.-W. Ohk, W.-C. Zin, J.-H. Lee and T.-K. Kim, *J. Mater. Chem.*, 2010, **20**, 3743–3749.
18 E.-J. Choi, E.-C. Kim, S.-B. Park, W.-C. Zin, Y.-J. Lee and J.-H. Kim, *J. Mater. Chem.*, 2012, **22**, 24930–24935.
19 N. Gimeno, M. J. Clemente, P. Forcén, J. L. Serrano and M. B. Ros, *New J. Chem.*, 2009, **33**, 2007–2014.
20 I. Alonso, J. Martinez-Perdiguero, J. Ortega, C. L. Folcia, J. Etxebarria, N. Gimeno and M. B. Ros, *Liq. Cryst.*, 2010, **37**, 1465–1470.
21 J. Watanabe, T. Niori, T. Sekine and H. Takezoe, *Jpn. J. Appl. Phys.*, 1998, **37**, L139–L142.
22 J. Martinez-Perdiguero, J. Etxebarria, C. L. Folcia, J. Ortega, N. Gimeno and M. B. Ros, *Phys. Rev.E: Stat., Nonlinear, Soft Matter Phys.*, 2010, **82**, 0417061–0417067.
23 D. A. Coleman, C. D. Jones, M. Nakata, N. A. Clark, D. M. Walba, W. Weissflog, K. Fodor-Csorba, J. Watanabe, V. Novotna and V. Hamplova, *Phys. Rev. E: Stat., Nonlinear, Soft Matter Phys.*, 2008, **77**, 0217031–0217036.
24 A. Yamaguchi, M. Watanabe and A. Yoshizawa, *Liq. Cryst.*, 2007, **34**, 633–639.
25 Y. Naito, R. Ishige, M. Itoh, M. Tokita and J. Watanabe, *Chem. Lett.*, 2008, **37**, 880–881.
26 K. Yamada, E. W. Lee, M. Hattori, S. Kawauchi, E.-J. Choi, J. Watanabe and S. Kang, *J. Mater. Chem. C*, 2014, **2**, 10418–10427.
27 H. Nguyen, S. Kang, M. Tokita and J. Watanabe, *Jpn. J. Appl. Phys.*, 2011, **50**, 0716021–0716024.
28 S. Kang, H. Nguyen, S. Nakajima, M. Tokita and J. Watanabe, *Phys. Rev. E: Stat., Nonlinear, Soft Matter Phys.*, 2013, **87**, 0525011–0525017.
29 R. A. Reddy, C. Zhu, R. Shao, E. Korblova, T. Gong, Y. Shen, E. Garcia, M. A. Glaser, J. E. Maclennan, D. M. Walba and N. A. Clark, *Science*, 2011, **332**, 72–77.
30 See ESI: POM micrographs of SmA phase without (Fig. S1a) and with compensator (Fig. S1b).†
31 See ESI: POM micrographs of B7 phase without (Fig. S1c) and with compensator (Fig. S1d).†
32 Y. Arakawa, S. Nakajima, R. Ishige, M. Uchimura, S. Kang, G. Konishi and J. Watanabe, *J. Mater. Chem.*, 2012, **22**, 8394–8398.
33 S. Kang, S. Nakajima, Y. Arakawa, M. Tokita, J. Watanabe and G. Konishi, *Polym. Chem.*, 2014, **5**, 2253–2258.
34 Molecular structure optimization was performed for N(1,7)–EIE–S1 by using density functional theory (DFT) with ωB97X-D/6–31G(d) method. The resulting dihedral angles around ester and Schiff's base moieties were set to 60° and −40°, respectively. Then, alkylthio tails were extended to $n = 16$ with all-trans zig-zag conformation with their plane parallel to that of neighbouring phenyl ring to calculate polarisation values and molecular length.
35 M. F. Vuks, *Opt. Spektrosk.*, 1966, **20**, 361–364.
36 J. Li and S. T. Wu, *J. Appl. Phys.*, 2004, **96**, 6253–6258.
37 See ESI: (*a*) Transmittance spectrum observed for fan-shape domain in SmA phase for N(1,7)–EIE–S16 black solid circle and the fitted value (red open square) by determination of Cauchy's coefficients; (*b*) Wavelength dispersion of obtained birefringence ($\Delta n'$).†
38 M. Lee, D. W. Lee, B. K. Cho, J.-Y. Yoon and W.-C. Zin, *J. Am. Chem. Soc.*, 1998, **120**, 13258–13259.
39 X. Cheng, X. Bai, S. Jing, H. Ebert, M. Prehm and C. Tschierske, *Chem.–Eur. J.*, 2010, **16**, 4588–4601.
40 M. Kölbel, T. Beyersdorff, X. H. Cheng, C. Tschierske, J. Kain and S. Diele, *J. Am. Chem. Soc.*, 2001, **123**, 6809–6817.
41 X. Li, S. K. Lee, S. Kang, M. Tokita, S. Kawauchi and J. Watanabe, *Chem. Lett.*, 2009, **38**, 424–425.
42 E. W. Lee, K. Takimoto, M. Tokita, J. Watanabe and S. Kang, *Angew. Chem., Int. Ed.*, 2014, **53**, 8216–8220.
43 See ESI:Scheme 1. Synthetic procedure.†
44 See ESI: NMR and elemental analysis data.†